Ferroelectrics, 2001, Vol. 258, pp. 21–30
Reprints available directly from the publisher
Photocopying permitted by license only

LOCAL STRUCTURE AND VIBRATIONAL DYNAMICS IN $NiWO_4$

A. KUZMIN, J. PURANS, R. KALENDAREV
Institute of Solid State Physics, University of Latvia, Kengaraga street 8, LV-1063 Riga, Latvia

(Received in final form April 15, 2001)

Systematic studies of nickel tungstate thin film, amorphous and polycrystalline powders were performed by X-ray absorption spectroscopy at the Ni K and W $L_{1,3}$ edges, X-ray diffraction and Raman spectroscopy. We found that in spite of the similarity of the local environment around nickel and tungsten ions in all three materials, there is strong difference in the Ni-O and W-O interactions for thin film/amorphous powder and polycrystalline powder. The nickel-oxygen bonding becomes stronger by going from thin film or amorphous powder to polycrystalline tungstate at the expense of the tungsten-oxygen bonding strength. Besides, in thin film and amorphous $NiWO_4$, nickel and tungsten ions have plane square-like $[NiO_4]O_2$ and nearly tetrahedral-like $[WO_4]O_2$ coordinations, whereas in polycrystalline $NiWO_4$ both ions have distorted octahedral-like $[Ni(W)O_4O_2]$ environment. The observed phenomena are related to the grain size effect.

Keywords tungstate; thin film; EXAFS; XANES; Raman spectroscopy; X-ray diffraction.

INTRODUCTION

Tungstates with the general formula AWO_4 are important materials, those properties depend strongly on the A^{2+}-cation type. For A^{2+}-cation being Ca^{2+}, Ba^{2+}, Sr^{2+} or Pb^{2+}, they have scheelite-type structure and are

widely used as solid-laser hosts, self-activated phosphors, scintillation detectors for X-rays and γ-radiation [1]. In the past, these materials have been studied mainly by optical spectroscopy: the origin of the self-luminescence was attributed to the $[WO_4]^{2-}$ groups but its mechanism is still unclear [2]. For A^{2+}-cation being Mg^{2+}, Cd^{2+} or 3d transition metal (from Mn^{2+} to Zn^{2+}), the structure becomes of wolframite-type. Some compounds of this group exhibit interesting magnetic properties related to A^{2+}-O^{2-}-A^{2+} superexchange interaction.

The scheelite structure may be regarded as a cubic close-packed array of A^{2+} and $[WO_4]^{2-}$ units with the coordination numbers of 8 and 4 oxygen atoms for the A^{2+} and W^{6+} cations, respectively, whereas the wolframite structure may be described as made up of hexagonally close-packed oxygens with certain octahedral sites filled by A^{2+} and W^{6+} cations in an ordered way [3]. An occurrence of the scheelite/wolframite-type structure depends mainly on the A^{2+}-cation size, but other factors, e.g. grains size or defects concentration, can play an important role too.

Among different AWO_4 compounds, nickel tungstate is of particular interest because of its antiferromagnetic (the Néel temperature $T_N \sim 67$ K) [2] and electrochromic [4] properties. The antiferromagnetism of $NiWO_4$ is related to the spin-spin interactions between $Ni^{2+}[3d^8]$ (S=1) ions, whereas the electrochromic effect is associated with a change of the tungsten ions valence state from W^{6+} to W^{5+} upon electrons injection [4]. In this work, we present the study of the local structure and vibrational dynamics in $NiWO_4$ by three complementary techniques – X-ray absorption spectroscopy (XAS), X-ray diffraction (XRD) and Raman spectroscopy.

EXPERIMENTAL AND DATA ANALYSIS

Amorphous green a-$NiWO_4$ powder was prepared by co-precipitation from nickel nitrate and sodium tungstate aqueous solutions at room temperature (RT). Polycrystalline brown $NiWO_4$ was obtained by thermal treatment of a-$NiWO_4$ at 700°C during 1 hour in the air.

Transparent thin films with a thickness ~1 μm were deposited on non-heated glass substrate by simultaneous reactive dc magnetron sputtering of W and Ni metal targets in Ar/O_2 atmosphere. The thin films show good electrochromic activity, probed by cyclic voltammetry measurements [4], and their surface morphology was determined by

atomic force microscopy (AFM), which suggests the presence of grains, having 60-120 nm size [4].

The RT X-ray absorption spectra of the Ni K and W $L_{1,3}$ edges were recorded at the LURE DCI storage ring, operated at the energy 1.85 GeV and a maximum stored current 316 mA. A standard transmission scheme with a Si(331), Si(311) and Si(111) double-crystal monochromators and two ion chambers containing argon/air was used. The energy resolution was about 1-2 eV. The X-ray absorption spectra were analysed following standard method by the EDA software package [5,6]. The X-ray absorption near edge structure (XANES) and extended X-ray absorption fine structure (EXAFS) were singled out in conventional way [5,6], and the *ab initio* multiple-scattering (MS) FEFF6 code [7] was used for modelling the Ni K-edge EXAFS signals. Note that in the MS calculations we used complex Hedin-Lundqvist exchange-correlation potential [7] and account for the MS contributions up to the fourth order, i.e. single-, double- and triple-scatterings.

XRD patterns were recorded at RT on a Bragg-Brentano-type X-ray diffractometer equipped with conventional X-ray tube with copper anode (Cu K_α radiation). The Bragg peaks assignment was done by comparison with JCPDS-ICDD PDF card No. 150755 of monoclinic $NiWO_4$.

The RT Raman measurements were carried out in 90°-geometry using conventional macro-Raman set-up with an argon laser excitation at 514.5 nm (laser power was 80-220 mW and resolution – 2.5 cm^{-1}). The scattered radiation was analysed through double-grating monochromator and detected by photomultiplier tube, operated in photon counting mode.

RESULTS AND DISCUSSION

Several experimental methods, utilized in the present work, allow to probe separately the short-range (XAS) and long-range (XRD) atomic structure as well as the Ni-O (Ni K-edge XAS) and W-O (W $L_{1,3}$-edges XAS, Raman) bondings.

XRD results (Fig. 1) suggest that a-$NiWO_4$ is amorphous, the as prepared (fresh) and annealed at 450°C thin films have nanocrystalline $NiWO_4$ structure with $<\bar{1}11>$ preferential orientation, and $NiWO_4$ has monoclinic phase. These conclusions agree also with Raman and EXAFS data discussed below.

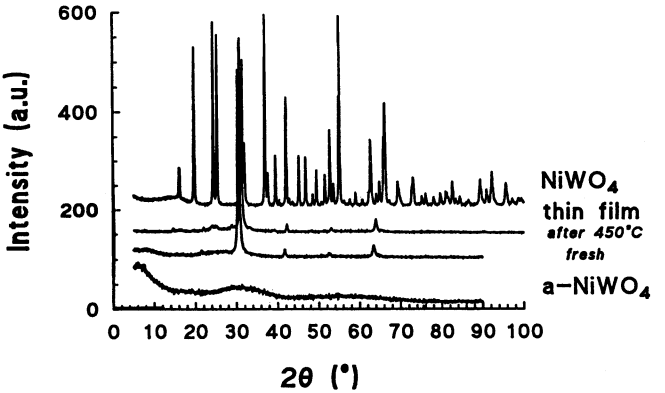

FIGURE 1: XRD patterns for nickel tungstate thin films (as prepared (fresh) and after annealing at 450°C), amorphous (lower curve) and polycrystalline (upper curve) powders.

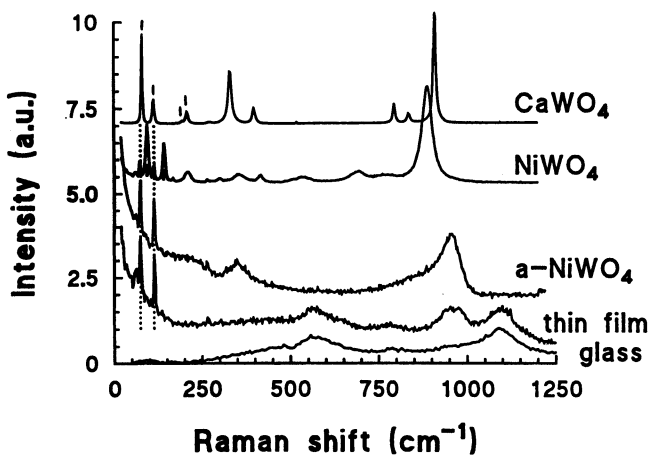

FIGURE 2: Raman spectra for nickel tungstate thin film, amorphous a-$NiWO_4$ and polycrystalline $NiWO_4$ powders. The spectra of polycrystalline $CaWO_4$ and of the thin film glass substrate are shown for comparison. Two vertical dashed lines indicate the low frequency modes typical for scheelite structure.

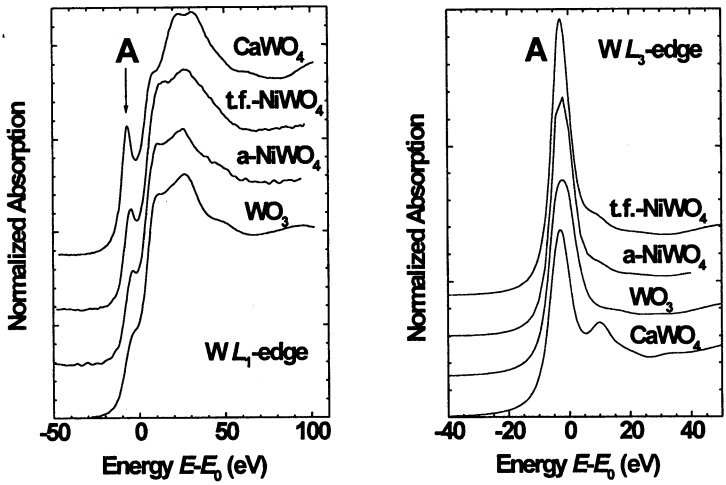

FIGURE 3: XANES at the W $L_{1,3}$-edges in thin film (t.f.) and amorphous (a) $NiWO_4$, polycrystalline WO_3 and $CaWO_4$.

The Raman spectra (Fig. 2) of tungstates reflect mainly tungsten sublattice, since nickel environment shows relatively week Raman activity. The modes assignment can be found, for example, in [8,9]. A peculiarity of the Raman spectra is the presence of a gap, which divides the external (<600 cm^{-1}) and internal (>600 cm^{-1}) modes of tungsten coordination polyhedra. The gap is clearly visible for tetrahedral tungsten coordination in $CaWO_4$ and becomes less defined for octahedral coordination of tungsten ions in polycrystalline c-$NiWO_4$. For thin film and amorphous $NiWO_4$, the separation of the modes is smeared because of a contribution of the glass substrate (the bands at 550, 800 and 1100 cm^{-1} in the thin film Raman signal) and bands broadening, which is consistent with nanocrystalline and amorphous nature of the samples.

The two interesting results are observed: (1) the frequency of the highest stretching W-O mode at 850-950 cm^{-1} is the largest in thin film and the smallest in c-$NiWO_4$; (2) the low-frequency lattice modes (<200 cm^{-1}) in thin films and a-$NiWO_4$ are closer to those of $CaWO_4$ with tetrahedral tungsten coordination but not to those of c-$NiWO_4$, where tungsten ions have distorted octahedral environment. The first result is related to the variation of the W-O bonds strength, whereas the

second one provides with an evidence of the tetrahedral-like coordination of tungsten ions in both disordered samples.

The last result is also supported by the shape of the W $L_{1,3}$-edges XANES (Fig. 3). For comparison we used two polycrystalline compounds WO_3 and $CaWO_4$, where the tungsten ions are located in distorted $[WO_6]$ octahedral environment and in the regular $[WO_4]$ tetrahedra, respectively. The tetrahedral coordination of tungsten ions in $CaWO_4$ results in strong mixing of 5d(W) and 2p(O) orbitals and leads at the W L_1-edge to well visible pre-edge peak A, being due to the dipole-forbidden transition 2s(W)→5d(W). In WO_3, built of distorted $[WO_6]$ octahedra, the 5d(W)-2p(O) orbital mixing decreases, and the peak A occurs just as a shoulder. Note that it disappears completely in regular octahedral coordination [10]. Thus, the presence of the peak A at the W L_1-edge in thin films and amorphous $NiWO_4$ suggests tetrahedral-like coordination for tungsten ions. The W L_3-edge XANES (Fig. 3) is less sensitive to the local symmetry, because the strong resonance A, the so-called "white line", is due to the dipole-allowed transition $2p_{3/2}(W)\rightarrow 5d(W)$ [10]. However, a comparison of the fine structure above the white line (Fig. 3) shows that the XANES signals for the thin films and amorphous $NiWO_4$ have the shape, which is somewhere in between the XANES signals for polycrystalline $CaWO_4$ and WO_3.

The Ni K-edge XANES signals (not shown) allow to obtain complementary information on the character of the Ni-O bonding by studying the variation of the pre-edge peak, which corresponds to $|1s3d^{8+i}\underline{L}^{i}\rangle \rightarrow |\underline{1s}3d^{8+i}\underline{L}^{i-1}\rangle$ (i = 1,2) transition [11,12,13]. Here L^i denotes the oxygen 2p-orbitals having i-holes in the place of i-electrons back donated to the nickel 3d orbitals, and $\underline{1s}$ stands for a Ni 1s core hole. The change of the pre-edge peak intensity for several compounds is shown in Fig. 4 (the data for c-NiO and c-MgO:Ni were taken from [11] and for thin film t.f.-NiO from [12]): it is related to the variation in the covalency of the Ni-O bonding or more precisely to the change in the oxygen-to-nickel back charge transfer [13]. The higher intensity of the pre-edge peak indicates stronger covalency or larger charge transfer. It is clear from Fig. 4 that the pre-edge peak intensity variation is opposite to a change in the value of the stretching mode frequency υ(W-O): the pre-edge peak increases when the frequency υ(W-O) decreases. This means that a competition for electron charge occurs in Ni-O-W atomic chains, so that the Ni-O bonds become stronger at the expense of the W-O bonds.

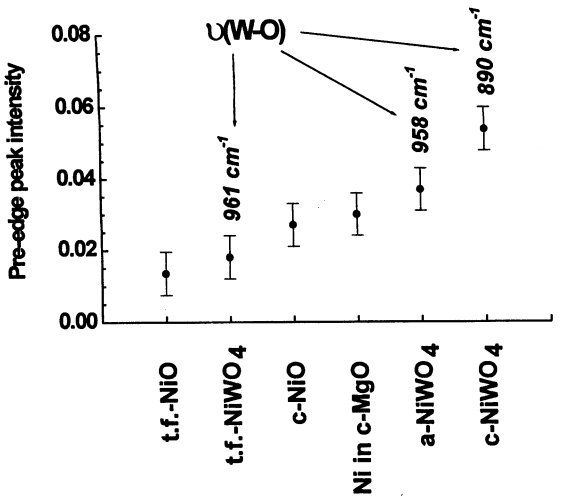

FIGURE 4: Variation of the pre-edge peak area at the Ni K-edge in several compounds. The highest stretching W-O mode frequencies from Raman spectra are also given.

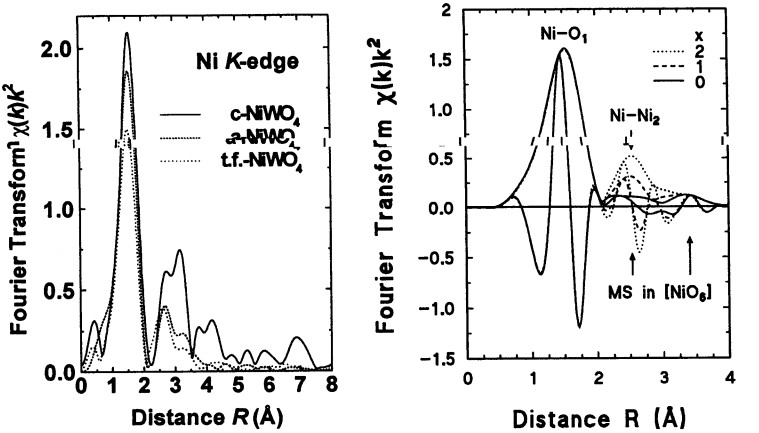

FIGURE 5: Left panel: Fourier transforms (FTs) of the Ni K-edge EXAFS signals in thin film (t.f.), amorphous (a) and crystalline (c) $NiWO_4$. Right panel: FTs of the calculated EXAFS signals for NiO_6Ni_x (x=0,1,2) clusters.

The change of the Ni-O bonds strength should be reflected by the variation of the local atomic structure around nickel ions, probed by the Ni K-edge EXAFS (Fig. 5, left panel). A comparison of the Fourier transforms (FTs) for thin film, amorphous and crystalline $NiWO_4$ allows to withdraw several conclusions. The thin film and amorphous $NiWO_4$ have similar but strongly disordered structure, so that only peaks up to about 4 Å are visible. The amplitude of the first coordination shell, the peak at 1.6 Å, changes in the same direction as the strength of the Ni-O bonds in Fig. 4. In fact, the first shell peak has higher amplitude for more covalent Ni-O bonding, that can be related to the smaller thermal and static disorder in polycrystalline tungstate.

The FTs for thin films and amorphous $NiWO_4$ can be compared to the model calculations, performed within multiple-scattering approach [7], for the small NiO_6Ni_x (x=0,1,2) clusters. The cluster represents a fragment of the local structure around nickel ions in polycrystalline $NiWO_4$. Six oxygen atoms, forming a regular octahedron, surround the central nickel atom. The remaining two nickel ions are connected to the central nickel via oxygens of the two opposite octahedron edges, located in the plane, formed by four oxygen atoms. Thus, the in-plane Ni-O-Ni angles are equal to 90°. The FTs of the calculated EXAFS signals are shown in Fig. 5 (right panel). The first peak at 1.5 Å is due to six nearest neighbour oxygen atoms. For x=0 (solid line), the two peaks at 2.5 and 3.5 Å correspond to the multiple-scattering contributions from the first shell octahedron [14]. For x=1 (dashed line) and x=2 (dotted line), an additional contribution from one and two nickel atoms, respectively, appears at 2.5 Å. Good qualitative agreement between calculated and experimental signals of thin film and a-$NiWO_4$ (Fig. 5) indicates that the NiO_6Ni_2 cluster is mainly responsible for their EXAFS signal.

More precise analysis of experimental Ni K-edge EXAFS signals shows that six oxygen atoms surrounding the central nickel ion, can be separated into two groups: 4 strongly bound in the plane with square-like arrangement and 2 weekly bound at the remaining vertices of an octahedron above and below the plane. The latter two oxygens are strongly bound to tungsten ions. Note also that no significant Ni-W contributions are observed in the Ni K-edge EXAFS signal that suggests weak interaction between the tungsten and nickel sublattices.

Thus, Raman and EXAFS results suggest that the interaction between nickel-oxygen and tungsten-oxygen polyhedra in the lattice is weak in the thin films and amorphous $NiWO_4$. Here the local

environment around nickel and tungsten ions can be described as tetrahedral-like $[WO_4]O_2$ or plane square-like $[NiO_4]O_2$. Note that in this model both tungsten and nickel ions are coordinated by six oxygen atoms but make a stronger bonding with only four of them. Such situation for tungsten ions represents an intermediate case between WO_3 and $CaWO_4$ compounds. In polycrystalline $NiWO_4$, the local environment of tungsten and nickel ions corresponds to distorted octahedral-like $[Ni(W)O_4O_2]$, and an increase (decrease) of the Ni-O (W-O) bond strength/covalency occurs compared to disordered compounds. Note that this type of local distortion around tungsten ions is close to that found in WO_3.

CONCLUSIONS

Systematic study using X-ray absorption spectroscopy, X-ray diffraction and Raman spectroscopy allowed us to obtain complete information on the structure of $NiWO_4$ system. The main result of the present work is that the Ni-O and W-O chemical bonding varies drastically depending on the size of $NiWO_4$ grains. The W-O bonds are stronger for small grains (i.e. in thin films and amorphous $NiWO_4$), whereas the Ni-O bonds are stronger for large grains (i.e. in polycrystalline $NiWO_4$). The change in the strength of the W-O and Ni-O bonding is accompanied by the modification of the local distortions around metallic ions.

Acknowledgements

J.P. is indebted to the LURE laboratory for providing the beam time and partial support. He is also grateful to Prof . S. Benazeth and Dr. Ph. Parent for assistance during XAS experiments. This work was supported in part by the Latvian Government Research Grant No. 96.0670.

References

1. Z.J. Kiss and R.J. Pressley, Proc. IEEE, **54**, 1236 (1966).

2. L.N. Limarenko, A.E. Nosenko, and M.V. Pashkovskii, Influence of Structural Defects on the Physical Properties of Tungstates. Visha Shkola, Lvov (1978) [in Russian].
3. A.W. Sleight, Acta Cryst. B, **28**, 2899 (1972).
4. A. Kuzmin, J. Purans, and R. Kalendarev, submitted to Electrochim. Acta.
5. A. Kuzmin, Physica B, **208&209**, 175 (1995); J. Physique IV (France), **7**, C2-213 (1997) <www http://www.dragon.lv/eda/>.
6. A. Kuzmin and J. Purans, J. Phys.: Condens. Matter, **12**, 1959 (2000).
7. J.J. Rehr, J. Mustre de Leon, S.I. Zabinsky, and R.C. Albers, J. Am. Chem. Soc., **113**, 5135 (1991); J. Mustre de Leon, J.J. Rehr, S.I. Zabinsky, and R.C. Albers, Phys. Rev. B, **44**, 4146 (1991).
8. H. Wang, F.D. Medina, Y.D. Zhou, and Q.N. Zhang, Phys. Rev. B, **45**, 10356 (1992).
9. D. Christofilos, S. Ves, and G.A. Kourouklis, Phys. Stat. Sol. (b), **198**, 539 (1996).
10. A. Kuzmin and J. Purans, J. Phys.: Condens. Matter, **5**, 9423 (1993).
11. A. Kuzmin, N. Mironova, and J. Purans, J. Phys.: Condens. Matter, **9**, 5277 (1997).
12. A. Kuzmin, J. Purans, and A. Rodionov, J. Phys.: Condens. Matter, **9**, 6979 (1997).
13. G. van der Laan, J. Zaanen, G.A. Sawatzky, R. Karnatak, and J.M. Esteva, Phys. Rev. B, **33**, 4253 (1986); M.A. van Veenendaal and G.A. Sawatzky, Phys. Rev. B, **50**, 11326 (1994).
14. A. Kuzmin and R. Grisenti, Phil. Mag. B, **70**, 1161 (1994).